Journal of Magnetic Resonance 282 (2017) 38–46

Contents lists available at ScienceDirect

Journal of Magnetic Resonance

journal homepage: www.elsevier.com/locate/jmr

Correction of environmental magnetic fields for the acquisition of Nuclear magnetic relaxation dispersion profiles below Earth's field

Vasileios Zampetoulas *, David J. Lurie [1], Lionel M. Broche [1]

Aberdeen Biomedical Imaging Centre, School of Medicine, Medical Sciences & Nutrition, University of Aberdeen, Foresterhill, AB25 2ZD, Aberdeen, United Kingdom

ARTICLE INFO

Article history:
Received 7 April 2017
Revised 14 July 2017
Accepted 20 July 2017
Available online 22 July 2017

Keywords:
Fast Field-Cycling MRI
T_1 dispersion
Ultra-low field applications
MRI contrast

ABSTRACT

T_1 relaxation times can be measured at a range of magnetic field strengths by Fast Field-Cycling (FFC) NMR relaxometry to provide T_1-dispersion curves. These are valuable tools for the investigation of material properties as they provide information about molecular dynamics non-invasively. However, accessing information at fields below 230 μT (10 kHz proton Larmor frequency) requires careful correction of unwanted environmental magnetic fields.

In this work a novel method is proposed that compensates for the environmental fields on a FFC-NMR relaxometer and extends the acquisition of Nuclear Magnetic Relaxation Dispersion profiles to 2.3 μT (extremely low field region), with direct application in the study of slow molecular motions. Our method is an improvement of an existing technique, reported by Anoardo and Ferrante in 2003, which exploits the non-adiabatic behaviour of the magnetisation in rapidly-varying magnetic fields and makes use of the oscillation of the signal amplitude to estimate the field strength. This increases the accuracy in measuring the environmental fields and allows predicting the optimal correction values by applying simple equations to fit the data acquired. Validation of the method is performed by comparisons with well-known dispersion curves obtained from polymers and benzene.

1. Introduction

Fast Field-Cycling (FFC) NMR relaxometry is a technique that measures relaxation times over a range of magnetic fields, most commonly the spin-lattice relaxation time T_1. The results acquired are presented in curves that indicate the dispersion of T_1 values (or alternatively the relaxation rates $R_1 = 1/T_1$) with the applied magnetic field or the corresponding Larmor frequency. These are known as T_1-dispersion curves or Nuclear Magnetic Relaxation Dispersion (NMRD) profiles and are used for the investigation of the molecular dynamics of a range of complex systems, with applications in various domains such as oil and polymer science, chemistry, biology or medicine [1–3].

An example of a pre-polarised FFC pulse sequence used for the acquisition of such curves is shown in Fig. 1. Such a pulse sequence measures the R_1 of the sample as a function of the evolution field B_0^E. This is achieved by repeatedly applying the sequence using identical polarisation and detection stages while varying the duration and field strength of the evolution stage. In this way, the decaying magnetisation is sampled point-by-point via the FID signals acquired and an exponential fit can be used to provide the R_1 corresponding to each B_0^E. The effect of the switching intervals on the evolution of the magnetisation does not bias the measurements of R_1, since the transition stages are applied identically for each B_0^E and the FID signals acquired are scaled by a constant factor [1,2,4].

FFC-NMR relaxometry typically ranges from 10 kHz to tens of MHz in proton Larmor frequency (PLF, equivalent to a range of 234 μT to hundreds of mT), depending on the hardware, probing molecular motions that range from sub-millisecond to nanosecond time scales [2]. However, in recent years there has been an increasing interest in its extension to the ultra- and even the extremely-low field region (ULF: 300 Hz–3 kHz PLF, equivalent to 7–70 μT; ELF: below 300 Hz PLF [5]) [6–8]. In these regimes, the direct relation between the correlation times probed and the Larmor frequency is not valid, because T_1 becomes comparable to the correlation times and the non-averaged local fields which originate from the dipolar couplings become comparable to B_0 [6]. Nevertheless, this extension is expected to provide insight into slower molecular dynamics than the ones probed when applying conventional FFC-NMR techniques [7,9].

FFC-NMR measurements extended to the ULF and ELF regions have previously been performed on water [4,7,10], industrial

* Corresponding author.
E-mail addresses: v.zampetoulas@abdn.ac.uk (V. Zampetoulas), d.lurie@abdn.ac.uk (D.J. Lurie), l.broche@abdn.ac.uk (L.M. Broche).
[1] DJL and LMB are joint senior authors of this paper.

http://dx.doi.org/10.1016/j.jmr.2017.07.008
1090-7807/

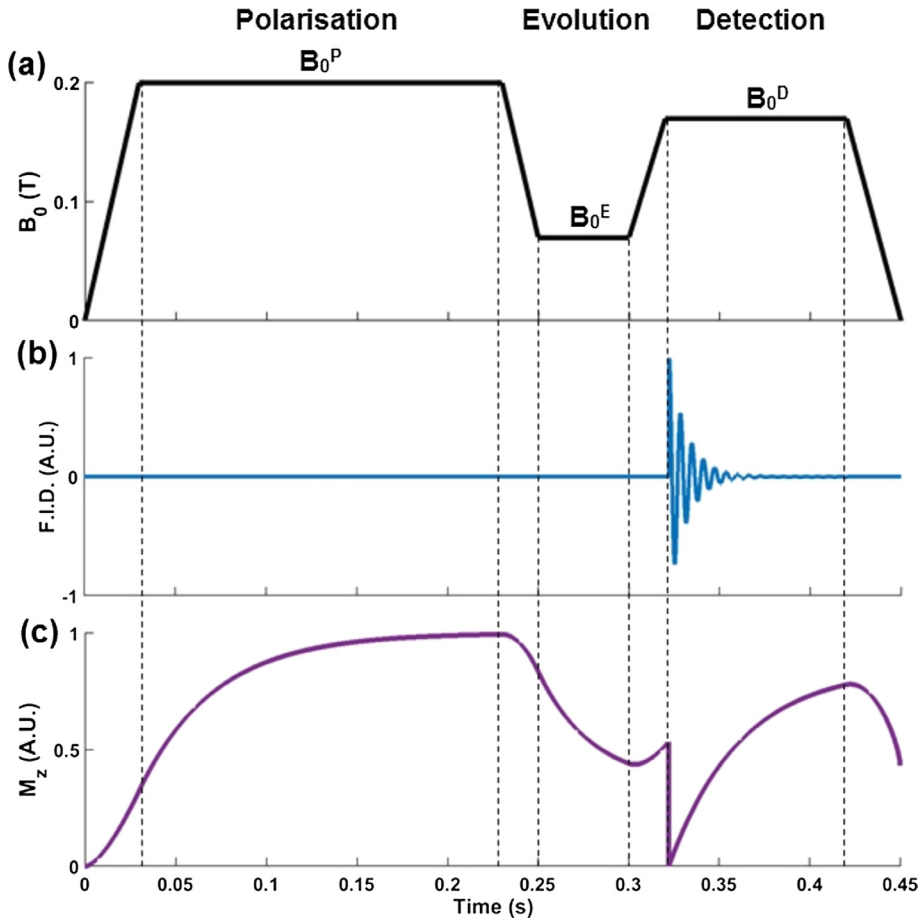

Fig. 1. A basic pre-polarised FFC pulse sequence, including (a) the variations of the applied magnetic field, (b) the FID signal generated after the application of a 90° RF pulse, and (c) the evolution of the magnetisation M_z. The dotted lines indicate the different stages of the pulse sequence and the field ramps between them. Note that the ramp times between field plateaux have been exaggerated, to emphasize the behaviour of the magnetisation.

chemicals [7,8] and a range of polymers [2,6,11–13], with the acquired results illustrating plateaux [7,13] and dispersions described by either Lorentzian [4,7,10] or power-law functions [6,11,12] in the extended regimes. In the domain of biomedical research, data at that range of fields is scarce, however NMRD profiles acquired from animal tissues [14–17], human breast, haemoglobin and red blood cells [15,18], as well as brain white and grey matter [18,19] ex vivo, show strong dispersion and contrast as the applied field extends down to 10 kHz PLF, indicating that the extension to the ULF region can potentially provide useful biological and clinical information.

The successful application of relaxometry below 10 kHz PLF requires precise correction of the unwanted environmental magnetic fields generated by a number of sources, including the Earth, electrical equipment and ferromagnetic structures in proximity to the magnet, since these set a limit on the FFC-NMR measurements when their magnitude becomes comparable to that of the evolution field [2,4,20]. When this situation occurs the results acquired depend on the orientation of the environmental fields. In the case when the angle between the polarisation and environmental field is (at least approximately) zero, the magnetisation decays exponentially as in a conventional FFC experiment (Fig. 1). This provides misleading results since the R_1-values measured gradually plateau to the value corresponding to the environmental field strength. If the angle is significantly larger than zero, the fast transition usually fulfils the non-adiabatic condition. This causes the magnetisation to oscillate, as described later, providing incorrect measurements of R_1 which appear as scattered points in the acquired curve.

The correction of environmental fields applied in MR studies typically involves the installation of the apparatus in a magnetically shielded room [21] or the use of external coils that apply opposing correction fields [1,2,4], while their efficiency is most commonly verified by measuring the residual fields with the use of magnetometers [8,9]. However, these require additional components that may be expensive, difficult to find off-the-shelf or impractical to implement on existing hardware. Additionally, magnetometers with nT accuracy, necessary for accurate measurements of the environmental fields, are either larger than the bore of NMR relaxometers (widths of 25–32 mm [22,23] compared to 12 mm for a typical FFC-NMR device respectively) or limited to measuring fields along the longitudinal axis [24].

In a different approach, the environmental fields are measured by measuring the amplitude of the FID signals while applying magnetic fields within the range of few hundred Hz PLF. In [20], Anoardo and Ferrante sample the behaviour of the magnetisation during the evolution stage after a non-adiabatic transition, exploiting the fact that T_1 becomes shorter as the field strength decreases so that a successful compensation corresponds to an FID signal of minimum amplitude. In [7], Kresse et al. verify the existence of unwanted fields applied on their home-built FFC system, based on abrupt decreases of the FID signals observed at certain fields amongst the whole range applied. While these are elegant methods, they may have drawbacks depending on the hardware used. First, small changes in the amplitudes of the FID signals can be difficult to resolve so it is hard to determine when the desired amplitude is achieved. Second, they lack a predictive model and

therefore require finding the optimal points semi-manually, which can be time consuming.

In this paper we propose a method derived from [20] where we measure the environmental fields by sampling the precession frequency of the magnetisation after a non-adiabatic transition, instead of the signal amplitude. This allows us to develop simple analytical models of the signal obtained so that one can use curve fitting techniques on the data acquired to determine the longitudinal and transverse correction fields. This overcomes the drawbacks of the previous method and increases the accuracy of the technique. Below we describe the method in detail and validate it by acquiring dispersion curves extended to ultra-low fields from samples of polymers and benzene with well-known dispersion characteristics. Finally, we illustrate the potential of ULF relaxometry in biology and medicine by acquiring extended NMRD profiles from samples of human cartilage.

2. Theory

Non-adiabatic evolution of the magnetisation occurs when the magnetic field varies over time scales that are shorter than the inverse of the resonant frequency of the system, as described by the equation:

$$D\theta/dt \gg \gamma B(\mathrm{t}) \tag{1}$$

where θ is the angle defined by the variation of the direction of the magnetic field over dt, γ is the gyromagnetic ratio of the nuclei (typically ^{1}H) and $B(\mathrm{t})$ is the magnitude of the magnetic field at time t. In a simple spin-½ system one can consider that when the main field $\boldsymbol{B}_0$ decreases non-adiabatically fast to the environmental field $\boldsymbol{B}_\mathrm{e}$ the magnetisation vector $\boldsymbol{M}$ does not follow the direction of $\boldsymbol{B}_0$ (Fig. 2a, b). Instead, it roughly maintains its initial magnitude and direction and, after the transition completes, it precesses around the direction of $\boldsymbol{B}_\mathrm{e}$ with angle θ at Larmor frequency γB_e, for time intervals determined by the rates R_1 and R_2 for the longitudinal and transverse component respectively (Fig. 2c) [25].

In practice the small field $\boldsymbol{B}_e$ is of unknown magnitude and direction and the general expression for the precession in the laboratory frame is:

$$M(t) = M_0 e^{-tR}\begin{bmatrix} [1-\cos(\gamma B_\mathrm{e} t)]\cos(\theta)\sin(\theta)\cos(\varphi) + \sin(\gamma B_\mathrm{e} t)\sin(\theta)\sin(\varphi) \\ [1-\cos(\gamma B_\mathrm{e} t)]\cos(\theta)\sin(\theta)\sin(\varphi) + \sin(\gamma B_\mathrm{e} t)\sin(\theta)\cos(\varphi) \\ \cos(\gamma B_\mathrm{e} t) + [1-\cos(\gamma B_\mathrm{e} t)]\cos(\theta)^2 \end{bmatrix} \tag{2}$$

where $M(\mathrm{t})$ is the magnitude of $\boldsymbol{M}$ at time t, M_0 is the magnitude of M before the non-adiabatic transition, θ and φ are the angles defining the orientation of $\boldsymbol{B}_e$ with respect to the z- and x-axis respectively, and R is used instead of both R_1 and R_2 since they are usually equal at very low fields. After the evolution stage finishes, a second non-adiabatic transition is required to reach the acquisition field and obtain the FID signal (Fig. 2d). That transition produces a longitudinal and transverse component again, ideally with the latter being directly detectable by the RF coil without having to use an excitation pulse. In practice though, the transverse components are not observed in our system, probably because of time-dependent field inhomogeneities due to Eddy currents that act as spoiler gradients during the field ramps. Therefore we will not consider the transverse component at readout, though it could be used to determine the angle φ without having to make additional measurements [20]. At final, the amplitude of the FID signal generated is directly proportional to the magnitude of the longitudinal component of $\boldsymbol{M}$, M_z, given by:

$$M_z(\mathrm{t}) = \cos(\theta)^2 + \cos(\gamma B_e t)[1-\cos(\theta)^2] \tag{3}$$

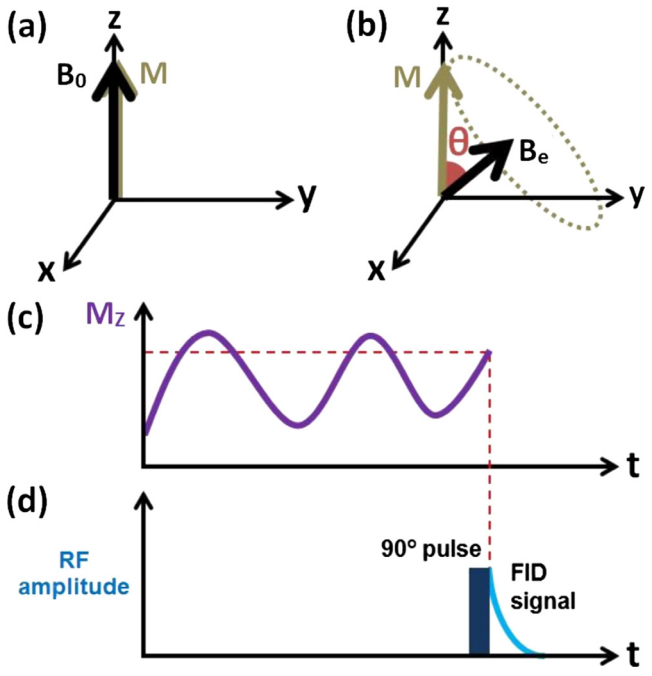

Fig. 2. The non-adiabatic transition in the laboratory frame for a spin-½. (a) Initial situation: the magnetisation M is aligned with the field B_0. At this stage, B_e is considered negligible. (b) Final situation: B_0 has switched non-adiabatically to 0 T and M precesses around B_e with an aperture angle θ. (c) M_z oscillates at Larmor frequency γB_e (typically below 5 kHz) around its equilibrium value (which is usually negligible). (d) The measurement of M is done after a known time by applying a 90° RF pulse. Repeated measurements for a range of precession times provide the precession frequency and therefore the magnitude of B_e.

where t is the time during the evolution stage.

During the precession of $\boldsymbol{M}$, the amplitude of the FID signal, and hence of M_z, oscillates with a frequency that is directly proportional to the strength of the environmental magnetic field (Fig. 2c). One can therefore make repeated measurements for a range of evolution times to measure the magnitude of the field by applying a Fast Fourier Transform on the amplitude of the FID amplitude signal (Fig. 2d).

It is also useful to derive models for the resultant field $\boldsymbol{B}_\mathrm{r}$ when a correction field $\boldsymbol{B}_\mathrm{c}$ is applied in addition to $\boldsymbol{B}_\mathrm{e}$. For practical reasons we split $\boldsymbol{B}_\mathrm{r}$ into the longitudinal and transverse components, $\boldsymbol{B}_\mathrm{r}^\mathrm{l}$ and $\boldsymbol{B}_\mathrm{r}^\mathrm{t}$ respectively. The magnitude of $\boldsymbol{B}_\mathrm{r}$ can then be expressed by:

$$B_\mathrm{r} = \sqrt{B_\mathrm{r}^{\mathrm{l}2} + B_\mathrm{r}^{\mathrm{t}2}} \tag{4}$$

with:

$$B_\mathrm{r}^\mathrm{l} = B_\mathrm{e}^\mathrm{l} + B_\mathrm{c}^\mathrm{l} \tag{5}$$

and:

$$B_\mathrm{r}^\mathrm{t} = \sqrt{[B_\mathrm{e}^\mathrm{t}\cos(\varphi) + B_\mathrm{c}^\mathrm{t}\cos(\varphi_\mathrm{c})]^2 + [B_\mathrm{e}^\mathrm{t}\sin(\varphi) + B_\mathrm{c}^\mathrm{t}\sin(\varphi_\mathrm{c})]^2} \tag{6}$$

where the superscripts l and t stand for the longitudinal and transverse components of the fields respectively and φ_c is the azimuthal angle of the correction fields.

3. Materials and methods

3.1. Materials

The FFC experiments described in this section were performed on a commercial bench-top FFC-NMR relaxometer (SMARtracer, Stelar S.r.l., Italy). This device can measure NMRD profiles of sam-

ples of up to about 1 mL at a wide range of temperatures, with the main field applied varying from 0 to 10 MHz PLF (234 mT). Voltage measurements across the terminals of the magnet, necessary to compensate for the existing voltage bias, were performed using a high-precision DC voltmeter (34420 A, Keysight Technologies, Santa Rosa, CA), and the measurements of the longitudinal fields were made using a fluxgate magnetometer (FLC 100, Stefan Mayer Instruments, Germany) connected to an oscilloscope (DSO-X-2024 A, Keysight Technologies, Santa Rosa, CA). The experiments for the correction of the environmental fields were performed using a 1-mL solution of 0.5 mM $MnCl_2$ at room temperature. This sample was chosen because it generated sufficient SNR and was convenient for experimentation due to its long R_1 and relatively low dispersion (about 6 and 30 s^{-1} at the polarisation and ultra-low fields respectively).

NMRD profiles were acquired from samples of the polymers polybutadiene (PB, M_w: 87,500 and 200,000, 0.61 and 1.04 g respectively), polyethylene oxide (PEO, M_w: 100,000 and 5,000,000, 0.4 g each), polydimethylsiloxane (PDMS, M_w: 110,000, 0.66 g), and polyisoprene (PIP, M_w: 38,000, 0.66 g), as well as of benzene (M_w: 78, 1 mL). The polymers were purchased from Sigma-Aldrich Ltd. (U.K.), apart from PB with Mw: 87,500 which was kindly provided to us by Prof. Ernst Rössler, Bayreuth University (senior author of reference [6]), while benzene was purchased from Fisher Scientific Ltd. (U.K.). The polymers were expected to generate NMRD profiles of constant slope below 10 kHz PLF [6,11,12] until B_0 became comparable to the existing non-averaged local fields, estimated at around 100 Hz PLF [26]. Benzene is known to have negligible dipolar coupling and was expected to generate NMRD profiles with very short R_1-values at room temperature (<0.5 s^{-1}) without any dispersion [8]. Due to these expected behaviours, the particular NMRD profiles were used to validate the correction of the environmental fields for a range of different evolution times, since deviations indicated the existence of a residual field which corrupted the acquisitions.

Additionally, NMRD profiles obtained from core samples of human cartilage were used as proof-of-concept for ULF contrast. The samples were extracted from the femoral heads of two female patients, both aged 79 years, who had undergone surgery at Aberdeen Royal Infirmary (Aberdeen, UK) for hip replacement due to osteoporosis. The patients did not show signs of osteoarthritis based on the results obtained from X-ray examination although there was mild wear. Two samples from each patient were used in total (10 mm diameters, 3 mm thicknesses, with minor impurities from subchondral bone), extracted from the femoral heads within six hours after surgery and stored at 4 °C for up to five days until the experiments were performed. Before storage, they were soaked in Fluorinert (FC-40, Sigma Aldrich) in order to maintain their moisture and structure without affecting the results of the FFC experiments. The femoral heads were provided by the NHS Grampian Biorepository (Aberdeen Royal Infirmary, Foresterhill, Aberdeen, AB25 2ZN, UK), and ethical approval for the study was granted by Health Improvement Scotland (REC Reference 16/NS/0055).

Analysis and plotting of the data, as well as curve fitting, was performed in MATLAB R2013a (The Mathworks, Natick, MA).

3.2. Preliminary work

Prior to the method of correction, particular efforts were made to reduce the effects of unwanted fields generated by equipment in proximity to the FFC magnet and by certain parts of the relaxometer. At first, to supress the influence of fields generated by electronic devices in operation and by eddy currents flowing in ferromagnetic materials, equipment such as the heat transfer system and the aluminium casing of the relaxometer were removed when possible or placed as far as possible from the FFC magnet.

Then, the voltage bias applied across the terminals of the magnet was compensated, to suppress the current bias which flows through the magnet and affects B_0^E. This compensation involved repeated applications of the pre-polarised pulse sequence with an evolution field set at 0 T and evolution time longer than 1 s. During this process, the voltage bias during the evolution stage was measured precisely down to the range of μV, while the field correction was adjusted via the relaxometer software until the bias was suppressed within the range of about ±30 μV. This had to be repeated for each experiment below 10 kHz PLF to account for time-varying drifts of the bias.

The effect of this preliminary work on the environmental magnetic fields applied on the longitudinal plane was characterised using a fluxgate magnetometer placed in the bore of the FFC magnet after removing the probe RF coil to increase the space available.

3.3. Correction method

The correction method itself was performed separately for the longitudinal and transverse environmental fields. Both were performed using the pre-polarised pulse sequence with the correction fields $\boldsymbol{B}_c$ incremented automatically. The longitudinal correction field was generated by the main magnet as an offset to the main field B_0, while the transverse correction field was generated by two pairs of saddle coils which were provided by the manufacturer and were incorporated in the relaxometer to generate constant fields along the x- and y-axes. The relaxometer was designed to apply the pulse sequences with a field transition interval of 3 ms, which allowed for large non-adiabatic limit angle θ ($\approx$ 78°) and therefore generated FID signals of large amplitudes. The polarisation, relaxation and detection fields were set to 10, 0, and 7.4 MHz respectively, the polarisation time was set to 0.3 s, and the evolution time varied linearly by 30 increments, from 4 ms to 10 μs and from 8 ms to 20 μs for the longitudinal and transverse correction respectively. During the longitudinal correction process, the magnitude of the correction field varied from −23.5 to +4.7 μT, with a transverse correction field of 7 μT applied at an azimuth angle of 0° to increase the visibility of the precessing $\boldsymbol{M}$ at 0 T. In the transverse correction process, the azimuth angle of the correction field applied at 4.7 μT, varied from −180° to +180°. The variation in both processes was completed in 90 increments to enhance the precision of the curve-fitting procedure. The measurements at each increment were repeated 10 times to enhance the SNR and also to correct the phase errors, occurring due to the remaining field instabilities, by averaging the acquired FID signals.

The data acquired was processed using Matlab 2015a to obtain the resultant field and Eqs. (5) and (6) were applied to fit the acquired data and derive the optimal correction fields. In practice, it was necessary to scale the parameters B_c^l and B_c^t using the scaling factors p_l and p_t to account for non-ideal control of the field correction coils. Fitting the data with Eqs. (5) and (6) led to the measurement of B_e^l, B_e^t and φ. $\boldsymbol{B}_e$ was then compensated for by setting the constant correction fields $B_c^l = -B_e^l/p_l$ and $B_c^t = -B_e^t/p_t$ of azimuth angle $\varphi_c = \varphi - 180°$.

3.4. Validation

A useful way to validate the correction of the environmental field is to measure the frequency of precession of the magnetisation with the evolution field set to 0 T. This has been reported by other groups [7] and is a robust validation but it relies on the static nature of the residual fields. Our relaxometer generated fluctuating

residual fields which perturbed the measurements below 300 Hz PLF, and therefore alternative methods of validation were required.

Here we validate the correction by acquiring NMRD profiles from the samples of polymers and benzene. Each experiment on polymers had a duration of around 30 min, and was carried out at temperatures of 90, 80, 20 and 70 °C for the samples of PDMS, PB, PIP and PEO respectively, which were chosen to reproduce the experimental conditions described in previously reported studies [6,11,12]. The experiment on benzene had a duration of 3.5 h and was carried out at 20 °C, while each experiment on human cartilage had a duration of about 40 min and was carried out at 37 °C. NMRD profiles were acquired from all samples using an Inversion-Recovery Carr-Purcell-Meiboom-Gill (IRCPMG) pulse sequence with 512 echoes and an echo time of 30 μs. As the sequence only records one data point per echo the acquisition filter was lowered to 60 kHz. The polarisation and acquisition fields were set to 10 and 7.4 MHz PLF respectively. The polarisation times were set to 0.5, 5 and 0.7 s for the samples of polymers, benzene and cartilage respectively, values of about twice the respective T_1 at 10 MHz PLF, which were necessary to acquire the NMRD profiles with only one repetition of the FFC-NMR experiment. The evolution field was set to vary between 10 MHz and 100 Hz PLF, while for each field 12 evolution periods were used, chosen to vary logarithmically between 0.1 and four times the estimated relaxation time at that field. R_1 was estimated from a monoexponential model using the absolute magnitude of the data [27].

The models applied to fit the NMRD profiles acquired from polymers and human cartilage were a sum of piecewise power-law functions [2,11] and Lorentzian peaks [28]. Power law functions were applied to the NMRD profiles of polymers and human cartilage and had the form $R_1 = \sum_1^i a_i f^{-b_i}$, where each of the relaxation regimes indexed by i has a multiplication factor α and an exponent b, which correspond to a vertical offset and slope respectively when plotting the data in log-log scale. The Lorentzian functions were applied to fit the quadrupole peaks appearing in cartilage due to the transfer of magnetisation between ^{1}H and ^{14}N [28].

As mentioned above, fluctuations of the residual fields were observed. These were estimated from the Fourier transform of the magnetisation precession signal when adding a constant and well-defined transverse field bias to the correction values. The effect of fluctuations is to broaden the frequency peak, which provides an estimate of the amplitude of the fluctuations.

4. Results and discussion

4.1. Preliminary work

The high rates of B_0 switching between the stages of the pulse sequences (about 80 T/s) were found to induce eddy currents in the conductive parts of the hardware. These generated an unwanted field of about 41 μT at the beginning of the evolution stage, which decayed exponentially below 1 μT in 5.5 ms. Removing the conductive casing of the FFC magnet led to the decrease of the unwanted field to 5.3 μT at the beginning of the evolution stage, with the exponential decay below 1 μT occurring in 0.8 ms.

The voltage bias, if not calibrated, drifted to a maximum (or minimum) of ±150 μV within three hours of operation In addition, it showed additional fluctuations of ±10 μV every 0.5 s that peaked to ±30 μV every 3 s, although the specifications of the DC voltmeter used did not allow for further analysis of their frequency spectrum. The shifts of ±150 μV generated an unwanted field of about 5 μT, however by calibrating the bias they could be reduced by a factor of 5–15. The effect of these fluctuations on the evolution field could not be determined by the fluxgate magnetometer due to its finite resolution, although it is estimated that they caused the aforementioned phase errors.

4.2. Correction method

Fig. 3 plots the measurements of the resultant field B_r as functions of the longitudinal correction field B_c^l (Fig. 3a) and azimuth angle φ_c (Fig. 3b), along with the curves generated by fitting Eqs. (5) and (6) respectively. Each plot was acquired in about 6 h due to the 90 increments of each varying parameter and to the 10 repetitions of the measurements at each increment. In Fig. 3b, the values of B_r shown were smaller than those in Fig. 3a since they were measured after the correction of B_e^l. The quality of the curve fitting in both figures was very good ($R^2 > 0.99$) and provided a longitudinal environmental field B_e^l: 7.5 ± 0.4 μT with scaling factor p_l:

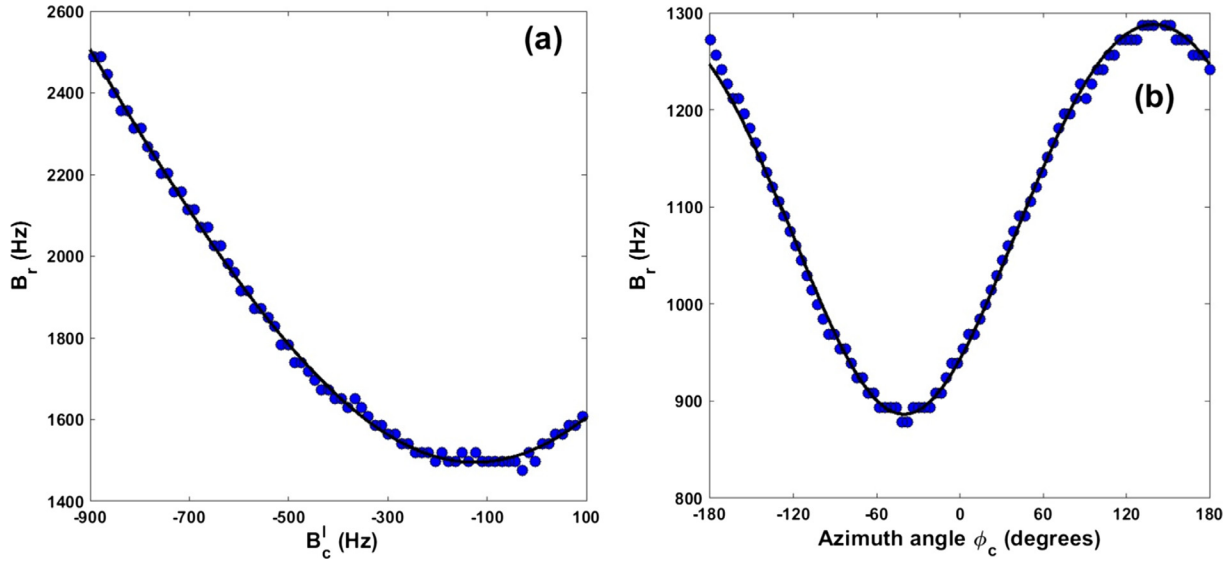

Fig. 3. Measurements of B_r plotted as a function of (a) B_c^l and (b) azimuth angle φ_c. The curves were generated by applying the Eqs. (5) and (6) to fit the data points shown in (a) and (b) respectively ($R^2 > 0.99$).

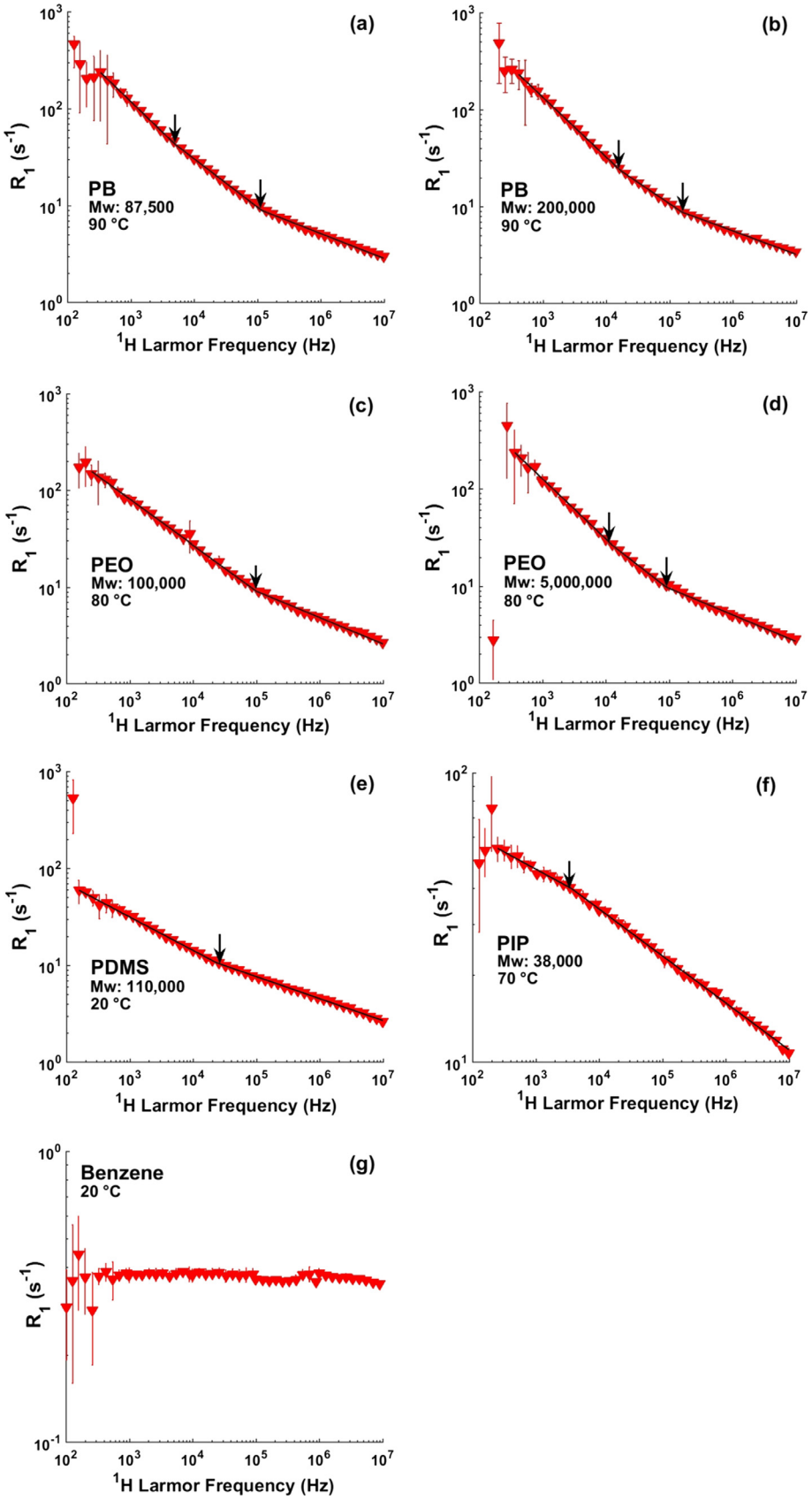

Fig. 4. NMRD profiles of the samples of PB with (a) Mw: 87,500 and (b) Mw: 200,000, PEO with (c) Mw: 100,000 and (d) 5,000,000, (e) PDMS, (f) PIP, and (g) Benzene, acquired with the environmental fields corrected. The arrows shown in the NMRD profiles of polymers illustrate the inflection frequencies between the different regimes.

Table 1
The vertical offset and slopes of each regime composing the NMRD profiles of the polymers, with the first regime being at the lowest and the last regime at the highest range of fields.

Polymer	Regime	Vertical offset (s^{-1})	Slope (unit-less)
PB (Mw: 87,500)	1st	1.5 ± 0.04	0.63 ± 0.004
	2nd	3.0 ± 0.2	0.5 ± 0.02
	3rd	5.2 ± 0.3	0.26 ± 0.04
PB (Mw: 200,000)	1st	1.8 ± 0.1	0.63 ± 0.01
	2nd	3.9 ± 1.0	0.45 ± 0.1
	3rd	5.6 ± 0.6	0.24 ± 0.1
PEO (Mw: 100,000)	1st	3.0 ± 0.1	0.474 ± 0.008
	2nd	4.9 ± 0.5	0.27 ± 0.09
PEO (Mw: 5,000,000)	1st	1.2 ± 0.1	0.62 ± 0.01
	2nd	2.9 ± 1.0	0.51 ± 0.1
	3rd	5.1 ± 0.8	0.27 ± 0.09
PDMS	1st	2.7 ± 0.05	0.356 ± 0.004
	2nd	4.4 ± 0.1	0.22 ± 0.01
PIP	1st	20.5 ± 0.5	0.118 ± 0.006
	2nd	16.0 ± 0.1	0.162 ± 0.001

2.6 ± 0.03 (a), and a transverse environmental field B_e^t: 4.7 ± 0.05 μT of scaling factor p_t: 5.5 ± 0.01 and azimuth angle φ: 139.7 ± 0.6° (b). Based on these measurements, the environmental fields were cancelled out by applying the opposing correction fields $B_c^l = -B_e^l/p_l = -2.9 \pm 0.2$ μT, and $B_c^t = -B_e^t/p_t = -0.85 \pm 0.01$ μT of azimuth angle $\varphi_c = \varphi - 180° = -40.3 \pm 0.6°$.

The results of the correction shown in this section were acquired after one application of the method. The magnitude and direction of the environmental fields, measured from two to four times per week during a period of three months, ranged from 6.0 to 8.4 μT for B_e^l, 4.7 to 7.0 μT for B_e^t and 103.7° to 154.5° for φ, with weekly variations that ranged from 0.1 to 1.5 μT for B_e^l, 0.1 to 1.2 μT for B_e^t and 3.4 to 38.6° for φ.

4.3. FFC-NMR applications extended to ULF

4.3.1. Polymers and benzene

The NMRD profiles obtained from the samples of polymers and benzene after the correction are shown in Fig. 4. The error bars shown indicate the 3-sigma error in R_1 from a monoexponential fit of the magnetisation amplitude. The power law models applied on the polymer profiles (Fig. 4a–f) were composed of two or three regimes as appearing in the literature [2,11] (Table 1: 2 regimes: PDMS, PIP and PEO; 3 regimes: PB; $R^2 > 0.99$). The regimes shown below 10 kHz PLF, where the effect of the correction appears, showed a constant slope down to minima of 330, 400, 260, 360, 160, and 250 Hz PLF (or 7.7, 9.3, 6.1, 8.4, 3.7 and 5.8 μT respectively) for PB (Mw: 87,500 and 200,000), PEO (Mw: 100,000 and 5,000,000), PDMS, and PIP respectively. Additionally, the NMRD profile of benzene (Fig. 4g) did not exhibit dispersion until the evolution field reached a minimum of 330 Hz PLF (7.7 μT). As the evolution field was lowered it reached a threshold value below which the size of the error bars increased dramatically (Fig. 4a–c) indicating the presence of non-adiabatic behaviour due to non-corrected or fluctuating local fields, which also caused the deviations from linearity shown in the non-fitted data points.

The presence of a fluctuating residual field after the application of the proposed correction method was verified by sampling the precession of the magnetisation using the sample of benzene, while applying an additional transverse field of 500 Hz (Fig. 5a, b). The frequency domain data (Fig. 5b) show a broad peak between 600–800 Hz, indicating time-varying field of roughly 100 Hz PLF amplitude, as well as a bias of the order of 200 Hz PLF.

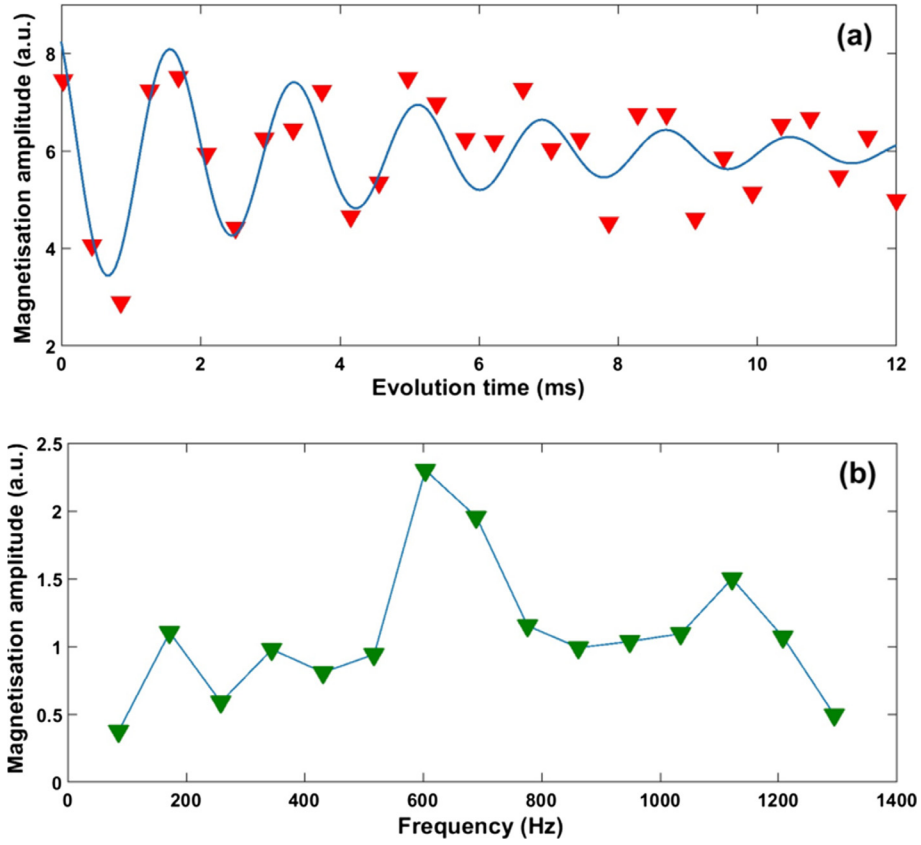

Fig. 5. The precession of M in the sample of Benzene during the evolution stage, in the (a) time and (b) frequency domain. The line in (a) is the fit of a cosine model with an exponential decay. The line in (b) is used to guide the eye.

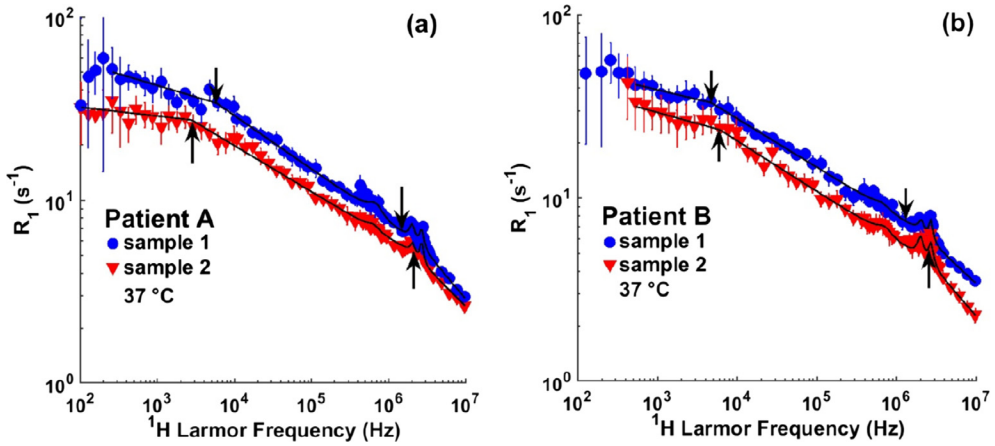

Fig. 6. NMRD profiles of the samples of cartilage, taken from different regions of the femoral heads of two patients, acquired with the environmental fields corrected. The arrows illustrate the inflection frequencies between the different regimes.

Table 2
The vertical offsets and slopes of each regime composing the NMRD profiles acquired from the samples of cartilage.

Patient	Sample	Regime[a]	Vertical offset (s^{-1})	Slope (unit-less)
A	1	1st	17.5 ± 1.4	0.13 ± 0.01
		2nd	7.3 ± 0.6	0.3 ± 0.02
		3rd	9.0 ± 4.3	0.4 ± 0.28
	2	1st	20.1 ± 1.7	0.05 ± 0.01
		2nd	6.2 ± 0.3	0.25 ± 0.01
		3rd	7.5 ± 2.6	0.42 ± 0.25
B	1	1st	18.9 ± 1.6	0.1 ± 0.01
		2nd	7.9 ± 0.3	0.26 ± 0.01
		3rd	8.6 ± 2.1	0.39 ± 0.2
	2	1st	11.3 ± 1.2	0.12 ± 0.01
		2nd	5.9 ± 0.3	0.28 ± 0.01
		3rd	7.3 ± 2.1	0.5 ± 0.24

[a] The 1st regime lies in the lowest, the 2nd in the middle, and the 3rd in the highest range of fields.

4.3.2. Human cartilage

The NMRD profiles obtained from the samples of human cartilage with the environmental fields corrected are shown in Fig. 6. The data fitted well to a power law distribution ($R^2 > 0.99$) composed of three different regimes indicating a similarity with the polymers, which is consistent with the known fibrous structure of cartilage (Table 2). One can also note the presence of three quadrupolar peaks between 0.4–0.9 MHz, and 1.5–3.5 MHz PLF, as observed in other studies [29,30]. Thanks to the correction, the acquisition could extend reliably below 500 Hz PLF (11.7 μT) and in one case as low as 100 Hz PLF (2.3 μT, ELF region), as shown in Fig. 6a. The size of the error bars was increased below 10 kHz PLF due to the decreased SNR, partially caused as a result of the small volume of the samples used, as well as to non-averaged local fields, which may be relatively strong in a rigid structure such as cartilage, and also as a result of uncompensated environmental fields. Nevertheless, the data acquired below 10 kHz PLF revealed the existence of a new regime, and therefore different type of motion, that could only be studied when measurements were made in the ULF region.

5. Conclusions

In this work, we have presented an improved approach of a method that corrects for the environmental magnetic fields acting on a commercial FFC-NMR relaxometer, and have demonstrated NMRD profiles extended to the ULF and even ELF region acquired from samples of polymers, benzene and human cartilage. Our approach led to a more precise determination of the environmental fields than the original method (errors smaller than ±0.5 μT and ± 2.0° compared to ±9.4 μT and ±5.0° reported in [20] for the magnitude and orientation respectively) which were cancelled out by applying opposing correction fields. This level of precision was achieved with the use of simple predictive models which allowed us to overcome the limitations of the original method.

The validation using NMRD profiles from samples of polymers and benzene showed that our method is reliable down to 10 μT (450 Hz PLF) in FFC-NMR measurements with evolution periods from about 3 ms to 3 s, as the results obtained compared favourably with the literature. The main drawbacks are the long acquisition time needed to acquire the graphs shown in Fig. 3 (about 12 h in total), the need to compensate precisely for the voltage bias so that one needs a precision voltmeter, the limited frequency resolution of the precessing magnetisation which limited the measurement precision of the resultant fields and hence the accuracy of the method, and the inability to deal with time-varying fields which limit the lowest field attainable.

Corrections of shorter duration (less repetitions and data points to acquire Fig. 3) and of increased precision at lower fields, which reach the non-averaged local fields of the samples examined, may be possible if the perturbing time-varying fields, estimated between 100 and 300 Hz PLF (Fig. 5), are damped. This can be achieved by shielding or by applying time-varying correction fields, within the limits set by the noise that the current-supply system generates. Nevertheless, this technique can be applied on pre-existing narrow-bore relaxometers with little modifications involved and may be automated using predictive algorithms to

shorten the duration of the process, thanks to the simple models used.

The NMRD profiles extended to ULF and ELF regions can be used to study slow molecular dynamics, with direct applications in polymer science [6,7] and potential use in medicine. In the cases of human cartilage, the NMRD profiles below 10 kHz Hz PLF revealed an additional regime of different vertical offset and slope, indicating that slower molecular dynamics can be studied. With further development, the differences observed between the profiles acquired, acquired at both low and high fields, may provide clinically relevant information about the wide range of molecular motions taking place in tissues and form the basis of new types of contrast in the developing field of FFC-MRI [3].

Acknowledgments

V.Z. acknowledges funding from EPSRC under grant number EP/J500045/1, "A UK Magnetic Resonance Basic Technology Centre for Doctoral Training". Aspects of the work were funded by EPSRC grant EP/K020293/1, "Zero-Field MRI to Enhance Diagnosis of Neurodegeneration". This project has also received funding from the European Union's Horizon 2020 research and innovation program under grant agreement No 668119, project "IDentIFY". The authors are grateful to Mr. G.P. Ashcroft and Dr. W. Mathieson for providing access to the biological samples used.

References

[1] E. Anoardo, G. Galli, G. Ferrante, Fast-field-cycling NMR: Applications and instrumentation, Appl. Magn. Reson. 20 (3) (2001) 365–404.
[2] R. Kimmich, E. Anoardo, Field-cycling NMR relaxometry, Prog. Nucl. Magn. Reson. Spectrosc. 44 (3–4) (2004) 257–320.
[3] D.J. Lurie, S. Aime, S. Baroni, N.A. Booth, L.M. Broche, C. Choi, G.R. Davies, S. Ismail, D.O. HOgain, K.J. Pine, Fast field-cycling magnetic resonance imaging, C. R. Phys. 11 (2) (2010) 136–148.
[4] F. Noack, NMR field-cycling spectroscopy: principles and applications, Prog. Nucl. Magn. Reson. Spectrosc. 18 (1986) 171–276.
[5] Nomenclature of the frequency and wavelength bands used in telecommunications, International Telecommunication Union - Radiocommunication Sector 2015;V.431-8.
[6] A. Herrmann, B. Kresse, J. Gmeiner, A.F. Privalov, D. Kruk, F. Fujara, E.A. Rössler, Protracted crossover to reptation dynamics: a field cycling 1H NMR study including extremely low frequencies, Macromolecules 45 (3) (2012) 1408–1416.
[7] B. Kresse, M. Becher, A.F. Privalov, M. Hofmann, E.A. Rössler, M. Vogel, F. Fujara, 1H NMR at larmor frequencies down to 3 Hz by means of field-cycling techniques, J. Magn. Reson. 277 (2017) 79–85.
[8] B. Kresse, A.F. Privalov, A. Herrmann, M. Hofmann, E.A. Rössler, F. Fujara, Simultaneous measurement of very small magnetic fields and spin-lattice relaxation, Solid State Nucl. Magn. Reson. 59–60 (2014) 45–47.
[9] B. Kresse, A.F. Privalov, F. Fujara, NMR field-cycling at ultralow magnetic fields, Solid State Nucl. Magn. Reson. 40 (4) (2011) 134–137.
[10] V. Graf, F. Noack, G.J. Béné, Proton spin T1 relaxation dispersion in liquid H2O by slow proton-exchange, J. Chem. Phys. 72 (2) (1980) 861–863.
[11] H.W. Weber, R. Kimmich, Anomalous segment diffusion in polymers and NMR relaxation spectroscopy, Macromolecules 26 (10) (1993) 2597–2606.
[12] S. Stapf, R. Kimmich, Field-cycling nuclear magnetic resonance relaxometry and field-gradient nuclear magnetic resonance diffusometry of polymers confined in porous glasses: Evidence for a restricted-geometry effect, Macromolecules 29 (5) (1996) 1638–1641.
[13] K.L. Seung, M. Mößle, W. Myers, N. Kelso, A.H. Trabesinger, A. Pines, J. Clarke, SQUID-detected MRI at 132 μT with T1-weighted contrast established at 10 μT-300 mT, Magn. Reson. Med. 53 (1) (2005) 9–14.
[14] R.G. Bryant, D.A. Mendelson, L.C. Coolbaugh, The magnetic field dependence of proton spin relaxation in tissues, Magn. Reson. Med. 21 (1) (1991) 117–126.
[15] S.H. Koenig, R.D. Brown, Relaxometry of tissue, John Wiley & Sons, 2007.
[16] S.H. Koenig, R.D. Brown III, Determinants of proton relaxation rates in tissue, Magn Reson Med 1 (4) (1984) 437–449.
[17] S.H. Koenig, R.D. Brown III, A molecular theory of relaxation and magnetization transfer: Application to cross-linked BSA, a model for tissue, Magn. Reson. Med. 30 (6) (1993) 685–695.
[18] S.H. Koenig, R.D. Brown III, M. Spiller, N. Lundbom, Relaxometry of brain: Why white matter appears bright in MRI, Magn. Reson. Med. 14 (3) (1990) 482–495.
[19] H.W. Fischer, P.A. Rinck, Y. Van Haverbeke, R.N. Muller, Nuclear relaxation of human brain gray and white matter: Analysis of field dependence and implications for MRI, Magn. Reson. Med. 16 (2) (1990) 317–334.
[20] E. Anoardo, G.M. Ferrante, Magnetic field compensation for field-cycling NMR relaxometry in the ULF band, Appl. Magn. Reson. 24 (1) (2003) 85–96.
[21] V.S. Zotev, A.N. Matlashov, P.L. Volegov, I.M. Savukov, M.A. Espy, J.C. Mosher, J. J. Gomez, R.H. Kraus Jr., Microtesla MRI of the human brain combined with MEG, J. Magn. Reson. 194 (1) (2008) 115–120.
[22] Keysight Technologies Inc. Keysight 34420A nano volt/micro ohm meter data sheet. Keysight Technologies Inc 2014.
[23] Mag-13 three-axis magnetic field sensor brochure. Bartington Instruments Ltd 2016.
[24] Stefan Mayer Instruments. Magnetic field sensor FLC 100 data sheet. Stefan Mayer Instruments 2016.
[25] B.F. Melton, V.L. Pollak, T.W. Mayes, B.L. Willis, Condition for sudden passage in the earth's-field NMR technique, J. Magn. Reson 117 (2) (1995) 164–170.
[26] J.P.C. Addad, NMR and fractal properties of polymeric liquids and gels, Prog. Nucl. Magn. Reson. Spectrosc 25 (1–3) (1993) 1–316.
[27] D.C. Montgomery, Design and analysis of experiments. 6th ed, John Wiley & Sons, USA, 2005.
[28] P.H. Fries, E. Belorizky, Simple expressions of the nuclear relaxation rate enhancement due to quadrupole nuclei in slowly tumbling molecules, J. Chem. Phys. 143 (4) (2015) 044202.
[29] L.M. Broche, G.P. Ashcroft, D.J. Lurie, Detection of osteoarthritis in knee and hip joints by fast field-cycling NMR, Magn. Reson. Med. 68 (2) (2012) 358–362.
[30] E. Rössler, C. Mattea, S. Stapf, NMR dispersion investigations of enzymatically degraded bovine articular cartilage, Magn. Reson. Med. 73 (5) (2015) 2005–2014.